ACS APPLIED MATERIALS & INTERFACES

Research Article

www.acsami.org

Highly Colloidally Stable Hyperbranched Polyglycerol Grafted Red Fluorescent Silicon Nanoparticle as Bioimaging Probe

Pradip Das and Nikhil R. Jana*

Centre for Advanced Materials, Indian Association for the Cultivation of Science, Kolkata-700032, India

Supporting Information

ABSTRACT: Here we report a surface modification approach for fluorescent silicon nanoparticle that transforms hydrophobic nanoparticle into water-soluble nanoparticle of high colloidal stability. The approach involves ring-opening polymerization of glycidol at the hydroxyl-terminated nanoparticle surface that results in a hyperbranched polyglycerol grafted silicon nanoparticle (Si-HPG). The resultant Si-HPG has 25 nm hydrodynamic diameter, low surface charge, and broad emission in the range of 450−700 nm with a fluorescence quantum yield of 6−9%. The Si-HPG has been transformed into cyclic RGD peptide functionalized nanoprobe using the conventional bioconjugation chemistry and used for specific targeting to $\alpha_v\beta_3$ integrin overexpressed cervical cancer cells and glioblastoma cells. Result shows that a silicon nanoparticle-based red fluorescent nanoprobe can be developed for *in vitro/in vivo* bioimaging applications.

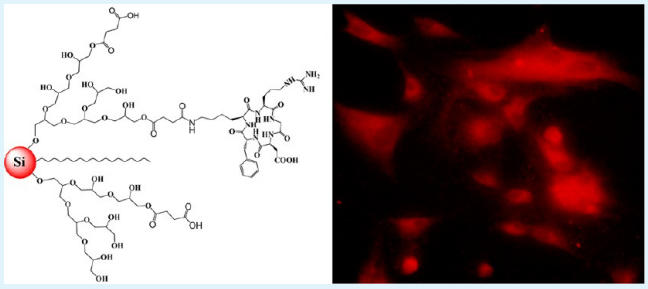

KEYWORDS: *silicon nanoparticle, red fluorescent probe, polyglycerol, RGD peptide, bioimaging*

INTRODUCTION

Red and near-infrared (NIR) fluorescent bioimaging nanoprobes enjoy all the advantage of nanometer length scale, provide options for deeper tissue imaging, and thus become more powerful in extracting information from a biological environment.[1−4] Important examples include fluorescent semiconductor nanoparticles (QDs) based probes,[5] fluorescent dye doped polymer beads[6] or silica nanoparticles,[7] doped semiconductor nanoparticle-based probes,[8] and fluorescent silicon nanoparticle-based probes.[9] Essential criteria to become an ideal nanoprobe include high photoluminescence quantum yield, high photostability, biocompatibility, optimum hydrodynamic size/shape, good colloidal stability under physiological condition and targeting options.[10,11] Among them widely used QDs-based nanoprobes have cadmium-based cytotoxicity issues,[12] and most of the nanoprobes have a charged surface that leads to high nonspecific binding problems in a biological environment.[11] Thus development of red/NIR fluorescent nanoprobe with high biocompatibility, high colloidal stability, and low nonspecific binding can greatly advance the biomedical research.

Fluorescent silicon nanoparticle-based probes are promising and fulfill most of the above criteria.[9,13] Silicon nanoparticles show tunable fluorescence of blue/green/yellow/red emission with reasonably high photoluminescence quantum yield and are highly biocompatibile.[13−16] However, the surface chemistry involving silicon nanoparticles is not well developed, and synthesis of water-soluble colloidally stable red/NIR fluorescent silicon nanoparticles remains an important challenge.[17] In earlier approach hydrophilic fluorescent silicon nanoparticles have been synthesized in the presence of hydrophilic ligands such as glutaric acid and immunoglobulin[18−20] or by surface functionalization of hydrophobic silicon nanoparticles with hydrophilic ligands[21−25] or coating of hydrophobic silicon nanoparticles with phospholipid micelles,[26−28] amphiphilic polymer,[29,30] poly(acrylic acid),[31] or lipid.[32] A large number of those studies used blue or green fluorescent silicon nanoparticles,[18,21−24,29,30] and very limited study is reported using red/NIR fluorescent silicon nanoparticles.[19,20,25−28,31−33] In fact there are only few reports on the synthesis of high quality red/NIR fluorescent silicon nanoparticles and their application in bioimaging.[19,20,26−28] In addition some studies show that red fluorescence of silicon nanoparticles becomes unstable during surface chemistry.[8,33] Nevertheless, these studies show that red/NIR fluorescent silicon nanoparticles can be a promising nontoxic bioimaging nanoprobe.

We are working on the development of nanoparticle-based fluorescent bioimaging probes,[11] and toward this direction we have synthesized a yellow/red fluorescent carbon nanoparticle-based probe,[34] a yellow fluorescent doped semiconductor nanocrystal-based probe,[35] and a green/yellow/red/NIR fluorescent silicon nanoparticle-based probe.[33] All of these reported nanoprobes have a charged surface that induces nonspecific interaction and lower colloidal stability in a biological environment. Herein, we report silicon nanoparticle-based yellow/red/NIR fluorescent nanoprobe with

Received: December 31, 2013
Accepted: February 20, 2014
Published: February 20, 2014

   dx.doi.org/10.1021/am406061x | ACS Appl. Mater. Interfaces 2014, 6, 4301−4309

low surface charge and superior colloidal stability. This nanoprobe is terminated with hyperbranched polyglycerol (HPG) and functionalized with peptide and has an average hydrodynamic diameter of 25 nm. HPG has hyperbranched polyol-like structures and thus is more hydrophilic in nature as compared to the well-known poly(ethylene glycol) (PEG) that has linear polyether-type stuuctures.[36] However, coating/grafting of HPG on the nanoparticle surface is less explored as compared to silica coating, polyacrylate coating, and other polymer coatings. Recently, various HPG-coated nanoparticles such as diamond, iron oxide, and quantum dot have been reported.[37−39] Herein we explore the grafting of HPG on hydrophobic silicon nanoparticles with the resultant formation of HPG-grafted silicon nanoparticle (Si-HPG). We have also demonstrated that hydroxy groups of HPG can be used for bioconjugation and functionalization with bioaffinity ligands for specific targeting applications. Combined with our reported simple and large scale benchtop synthesis for hydrophobic silicon nanoparticles,[33] this conversion approach will be very useful for the synthesis of various other silicon-based functional nanoprobes.

EXPERIMENTAL SECTION

Materials. Chloro(dimethyl)octadecylsilane, octadecylamine, glycidol, 4-dimethylamino pyridine (DMAP), triethylamine (Et_3N), 1-ethyl-3-(3-dimethylaminopropyl)carbodiimide hydrochloride (EDC), and *N*-hydroxy susccinimide (NHS) were purchased from Sigma-Aldrich. Succinic anhydride, 1,3,5-trimethylbenzene, dry dimethylformamide, and 1,2-dichlorobenzene were purchased from Spectrochem. Cyclo(Arg-Gly-Asp-D-Phe-Lys) peptide c(RGDfK) was purchased from GenPro Biotech.

Synthesis of Hydrophobic Silicon Nanoparticle. The hydrophobic silicon nanoparticle was prepared according to our previously reported low temperature thermal decomposition method.[33] Briefly, chloro(dimethyl)octadecylsilane (69.4 mg) and octadecylamine (6.7 mg) were dissolved in 12 mL of 1,3,5-trimethylbenzene and heated to 140 °C for 3 days in three necked flask under air atmosphere. Next, the solution mixture was cooled to room temperature, and hexane was added to precipitate the particles. The precipitate was collected and dispersed in chloroform, and this washing process was repeated several times. Finally, the precipitate was collected.

Synthesis of Hyperbranched Polyglycerol Grafted Silicon Nanoparticle (Si-HPG). About 10 mg of hydrophobic silicon nanoparticles was dispersed in 12 mL of 1,2-dichlorobenzene and heated at 140 °C under argon atmosphere. Then, 500 μL of glycidol dissolved in 2 mL of 1,2-dichlorobenzene was added dropwise within 15 min, and next the mixture was heated for 16 h under magnetic stirring. The resulting brownish gel was dissolved in methanol, and nanoparticles were precipitated by addition of acetone and separated via centrifugation. This process of methanol-induced redispersion and acetone-induced precipitation was repeated several times. Finally, the washed precipitate was dissolved in water and dialyzed against distilled water using a dialysis membrane (MWCO ∼2000 Da) to remove any free glycidol, methanol, and acetone.

Synthesis of Carboxylic Acid Functionalized Si-HPG Nanoparticle (Si-HPG-COOH). Si-HPG (200 mg) and 100 mg of succinic anhydride were dissolved in 10 mL of dry dimethylformamide. Next, 120 mg of DMAP and 1 mL of Et_3N were mixed and heated at 70 °C for 24 h under argon atmosphere. Under this condition the hydroxy groups of Si-HPG reacted with succinic anhydride. Next, the nanoparticles were precipitated by addition of acetone and collected via centrifugation. In order to remove excess reagents, the product was further dissolved in methanol and precipitated by addition of acetone. This process of methanol-induced dissolution and acetone-induced precipitation was repeated 3−4 times. Finally the product was dissolved in distilled water and dialyzed against distilled water using a dialysis membrane (MWCO ∼2000 Da) that removes excess reagents, methanol, and acetone.

Synthesis of Cyclic RGD Peptide Functionalized Si-HPG Nanoparticle (Si-HPG-RGD). About 2 mL of an aqueous solution of Si-HPG-COOH (10 mg/mL) was mixed with 200 μL of freshly prepared aqueous solution of 1-ethyl-3-(3-dimethylaminopropyl)-carbodiimide hydrochloride (20 mg/mL) and 200 μL of aqueous solution of *N*-hydroxy susccinimide (25 mg/mL). The pH of the solution was adjusted to 7.4 by adding PBS buffer, and solution was stirred for 30 min. Next, 500 μL of an aqueous solution of c(RGDfK) peptide (2 mg/mL) was added and stirred overnight. Next, excesses reagents and unbound peptide were removed by dialysis using a dialysis membrane (MWCO ∼2000 Da) against distilled water.

Arginine Determination. The presence RGD peptide bound with Si-HPG-RGD was determined by measuring the presence of arginine of RGD peptide by a previously reported method.[40] Briefly, 100 μL of Si-HPG, Si-HPG-COOH, or Si-HPG-RGD solution was mixed with 300 μL of an ethanolic solution of 9,10-phenanthrenequinone (150 μM) and 50 μL of NaOH solution (2 N). Next, the mixture was incubated at 60 °C for 3 h. Then, 200 μL of each sample was mixed with 200 μL of HCl (1.2 N), and the mixture was allowed to stand at room temperature under dark for 1 h. The emission of the mixture was measured at excitation wavelength 312 nm.

Cell Labeling and Imaging. Human cervical cancer HeLa cells and human glioblastoma U87MG cells were cultured in Dulbecco's modified eagle medium (DMEM) supplemented with 10% fetal bovine serum (FBS) and 1% penicillin/streptomycin at 37 °C and 5% CO_2. For cellular uptake studies, HeLa and U87MG cells were seeded into 4-well chamber slides. After overnight growth, Si-HPG, Si-HPG-COOH, and Si-HPG-RGD solutions were added to reach final concentrations of 0.5−1.0 mg/mL and incubated for 2−4 h. Next, cells were washed with PBS buffer solution, fixed with 4% paraformaldehyde, mounted with 50% glycerol, and used for microscopic studies.

Cytotoxicity Assays. The relative cytotoxic effect of the Si-HPG, Si-HPG-COOH, and Si-HPG-RGD nanoparticles was evaluated using conventional 3-(4,5-dimethylthiazol-2-yl)-2,5-diphenyltetrazolium bromide (MTT) based colorimetric assays. The HeLa and U87MG cells were seeded into 24-well plates at high density in DMEM media supplemented with 10% FBS and 1% penicillin/streptomycin at 37 °C and 5% CO_2. After overnight growth, the cells were incubated with nanoparticles of different final concentrations (0.1−2.5 mg/mL) for 24 h. Next, cells were washed with PBS buffer solution followed by addition of 500 μL of fresh DMEM medium to each well. Then, 50 μL of an aqueous solution of MTT (5 mg/mL) was added to each well and incubated for 4 h. The violet formazan was dissolved in sodium dodecyl sulfate (SDS) solution in a water/DMF mixture, and absorbance was measured at 570 nm using a microplate reader. The relative cell viability was measured assuming 100% cell viability for control cells without any nanoparticle.

Instrumentation. UV−vis absorption spectra were recorded on a Shimadzu UV-2550 UV−vis spectrophotometer, and fluorescence measurements were performed on a BioTek SynergyMx microplate reader. Transmission electron microscopy (TEM) images were obtained using a JEOL-JEM 2010 electron microscope. The field emission scanning electron microscopy (FESEM) image and elemental compositional analysis were performed with a Supra 40, Carl Zeiss Pvt. Ltd. instrument. The ^1H and ^{13}C NMR (500 MHz) spectra were recorded on a Bruker DPX-500 spectrometer at room temperature. Fourier transform infrared (FTIR) spectra of KBr powder-pressed pellets were recorded on a Perkin-Elmer Spectrum 100 FTIR spectrometer. X-ray photoelectron spectroscopy (XPS) measurement was performed using an Omicron (serial no. 0571) X-ray photoelectron spectrometer. Time correlated single photon counting (TCSPC) was performed through exciting the sample with picoseconds diode laser (IBH Nanoled) using a Horiba Jobin Yvon IBH Fluorocube apparatus. Thermogravimetric analysis (TGA) was performed using a TA SDT Q600 instrument. Dynamic light scattering (DLS) and zeta potential were measured using a NanoZS (Malvern) instrument. Fluorescence images and photostability of nanoparticles were performed by drop casting of sample solution on a

Scheme 1. Synthesis Strategy of Hyperbranched Polyglycerol Grafted Fluorescent Silicon Nanoparticles (Si-HPG) and Further Functionalization with Cyclic RGD Peptide

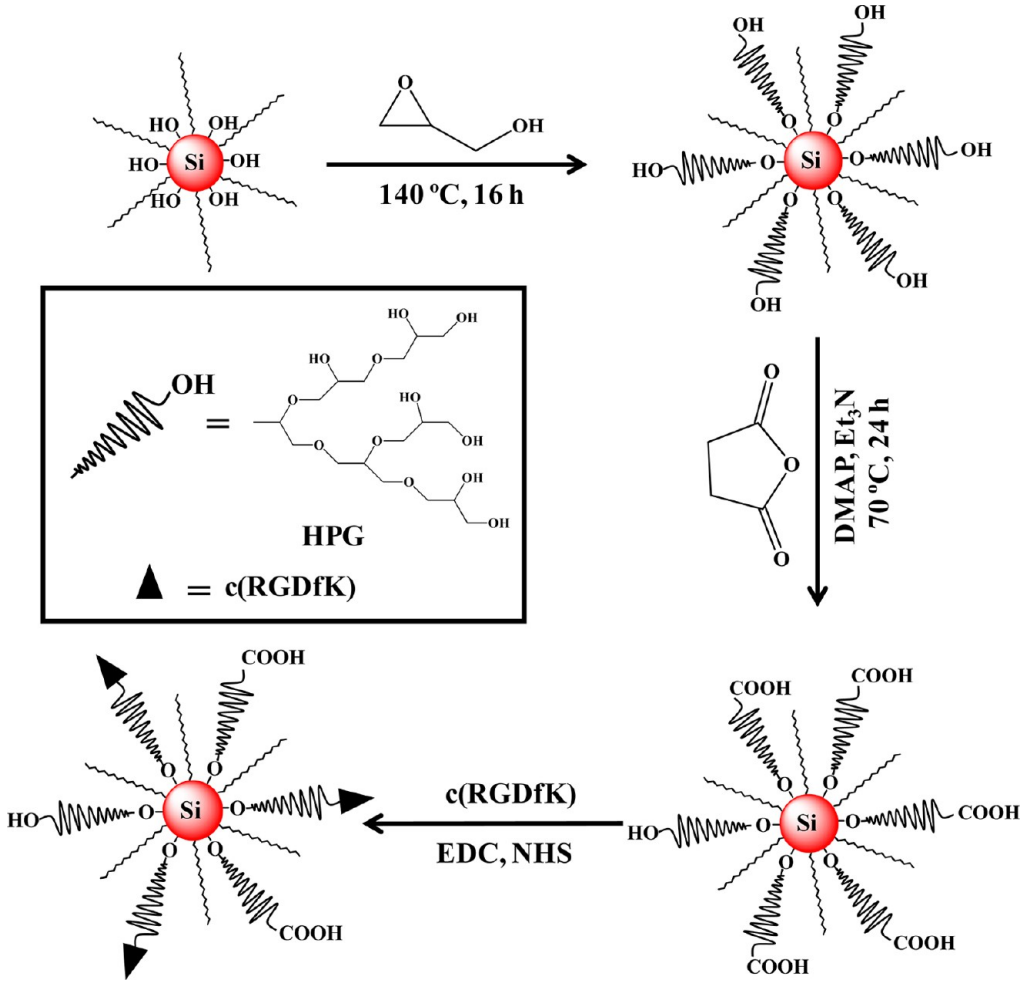

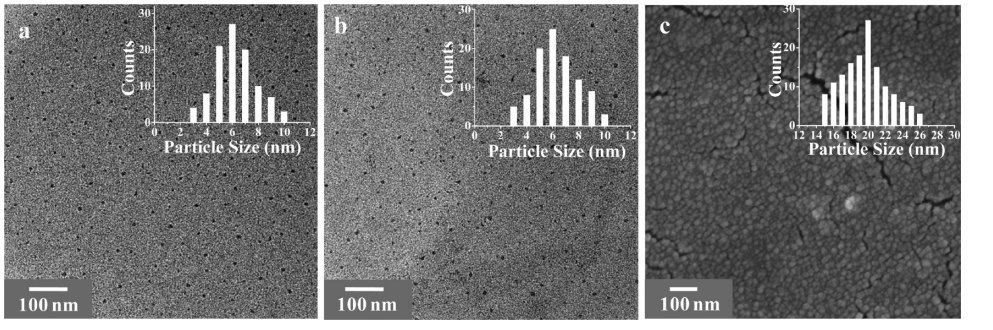

Figure 1. TEM images of hydrophobic silicon nanoparticles (a) and hydrophilic Si-HPG (b) and FESEM image of Si-HPG (c). Inset shows the size distribution of respective nanoparticles.

glass slide, and cell images were taken using an Olympus IX81 microscope. The differential interference contrast microscopy (DIC) and fluorescence images of cells were performed by Olympus IX81 microscope using image-pro plus version 7.0 software.

RESULTS AND DISCUSSION

Synthetic Strategy and Material Characterization. The synthesis strategy for Si-HPG is shown in Scheme 1 and involves ring-opening multibranching polymerization at the hydroxyl group terminated surface of hydrophobic silicon nanoparticles at 140 °C under argon atmosphere. The polymerization results in the grafting of HPG at the surface of the silicon nanoparticles and formation of water-soluble Si-HPG. At the next stage the terminal hydroxyl groups of Si-HPG are reacted with succinic anhydride, which results the formation of carboxylic acid terminated silicon nanoparticles (Si-HPG-COOH). Finally, 1-ethyl-3-(3-dimethylaminopropyl)-carbodiimide hydrochloride (EDC) coupling chemistry is used to prepare cyclic RGD peptide functionalized silicon nanoparticles (Si-HPG-RGD).

Figure 1 shows the transmission electron microscope (TEM) image of the silicon nanoparticles before and after HPG grafting. The hydrophobic silicon nanoparticles are spherical

dx.doi.org/10.1021/am406061x | ACS Appl. Mater. Interfaces 2014, 6, 4301−4309

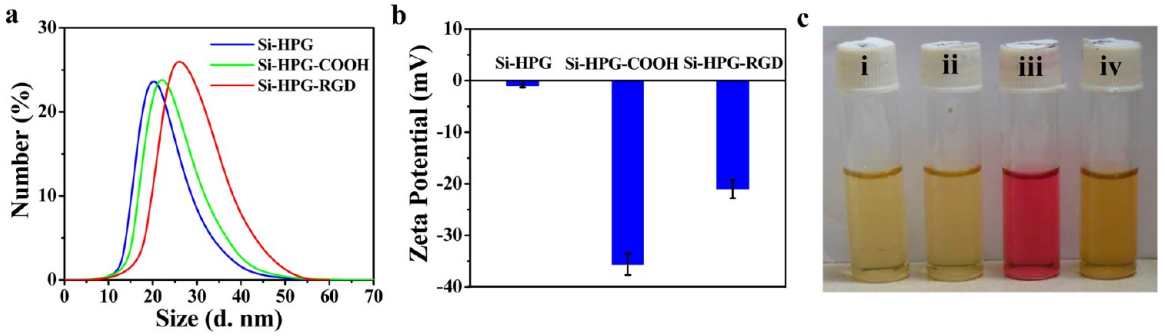

Figure 2. (a) Hydrodynamic sizes of Si-HPG, Si-HPG-COOH, and Si-HPG-RGD in pH 7.4 phosphate buffer showing the average hydrodynamic sizes of 22 ± 8, 23 ± 7, and 26 ± 8 nm, respectively. (b) The results of surface charge of Si-HPG, Si-HPG-COOH, and Si-HPG-RGD with the zeta potential values of −1 ± 0.3, −34.6 ± 2.1, and −21 ± 1.8 mV, respectively. (c) The colloidal stability of Si-HPG under different condition: (i) 1 M NaCl solution, (ii) pH 7.4 phosphate buffer, (iii) Dulbecco's modified eagle medium (DMEM) medium with 10% fetal bovine serum (FBS), and (iv) pure FBS.

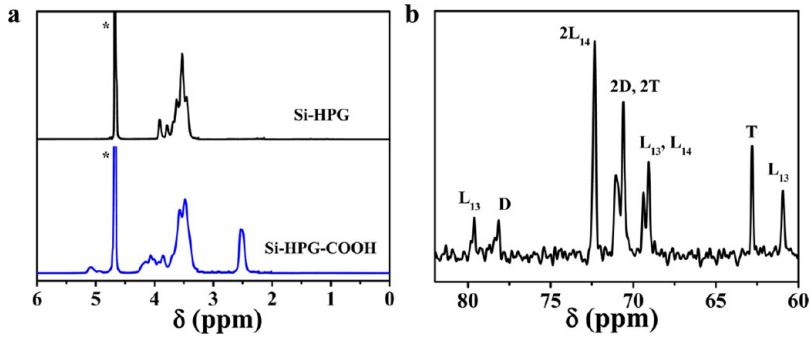

Figure 3. (a) ^{1}H NMR spectra of Si-HPG and Si-HPG-COOH in D_2O and (b) ^{13}C NMR spectrum of Si-HPG in D_2O. (∗ indicates residual solvent peak). Dendritic structure of HPG has been confirmed from ^{13}C NMR spectrum of Si-HPG with the characteristic peaks of terminal (T) carbon, dendritic (D) carbon, linear 1,3 carbon (L_{13}), and linear 1,4 carbon (L_{14}). For more detail see the description in the text.

with average diameter of 6 ± 2 nm. The TEM image of Si-HPG nanoparticles shows only the core silicon nanoparticles with unchanged diameter (Figure 1 and Supporting Information, Figure S1). Field emission scanning electron microscopy (FESEM) shows the estimated overall size of Si-HPG as 20 ± 2 nm, which includes both the core silicon particle and the HPG shell. This result concludes that the thickness of the HPG shell on the silicon nanoparticle surface is around 6 ± 2 nm. The corresponding energy dispersive X-ray (EDS) spectrum and elemental mapping clearly demonstrate that Si-HPG is composed of silicon, carbon, and oxygen (Supporting Information, Figure S2). In order to determine the amount of silicon present in Si-HPG, thermogravimetric analysis of Si-HPG was performed under nitrogen atmosphere (Supporting Information, Figure S3). The residue present for Si-HPG degradation even after 800 °C is ∼5%, which includes silicon/silicon oxide.

Dynamic light scattering (DLS) study was performed to determine the hydrodynamic size of the hydrophobic silicon nanoparticle, Si-HPG, Si-HPG-COOH, and Si-HPG-RGD (Figure 2 and Supporting Information, Figure S4). Results show that hydrodynamic size of hydrophobic silicon nanoparticles increases from 6 ± 2 to 22 ± 8 nm after HPG grafting. The substantial increased size of Si-HPG corroborates with the FESEM size of Si-HPG and further suggests efficient HPG grafting on the surface of silicon nanoparticles. The hydrodynamic sizes of the Si-HPG-COOH and Si-HPG-RGD are 23 ± 7 and 26 ± 8 nm, respectively. The relatively smaller size increase in the latter cases is due to the modification with small molecules and insignificant particle aggregation.

The surface charge of Si-HPG, Si-HPG-COOH, and Si-HPG-RGD was estimated from zeta potential measurement (Figure 2). The surface charge of Si-HPG is close to zero (typically in the range of −1 to −2 mV) and independent of pH. However, Si-HPG-COOH has negative surface charge (typically −35 mV at pH 7.4) due to the presence of carboxylate functional groups. The surface charge of Si-HPG-RGD is also negative (typically −21 mV) and decreased as compared to Si-HPG-COOH. Such decrease in surface charge is due to the conjugation with RGD peptides that consumes a fraction of the carboxylate groups.

The presence of HPG on the silicon nanoparticle surface and its chemical structure were confirmed by solution phase ^{1}H and ^{13}C NMR spectroscopy. The ^{1}H NMR spectrum of Si-HPG shows the characteristic proton signals of $-CH_2O-$ and $-CHO-$ units of HPG in the range of 3.4−4.0 ppm, and the active proton signal of multiple hydroxy groups of HPG is observed around 4.5 ppm, which overlaps with the residual solvent peak (Figure 3). The ^{13}C NMR spectrum of Si-HPG indicates that grafted HPG has an analogous dendritic structure. In the ^{13}C NMR spectrum, the characteristic peaks of terminal (T) carbon (at 62.85 ppm corresponding to CH_2OH and at 70.55 ppm corresponding to CHOH), dendritic (D) carbon (at 71.07 ppm corresponding to CH_2 and at 78.13 ppm corresponding to CH), linear 1,3 (L_{13}) carbon (at 60.9 ppm corresponding to CH_2OH, at 69.38 ppm corresponding to CH_2 and at 79.6 ppm corresponding to CH), and linear 1,4

dx.doi.org/10.1021/am406061x | ACS Appl. Mater. Interfaces 2014, 6, 4301−4309

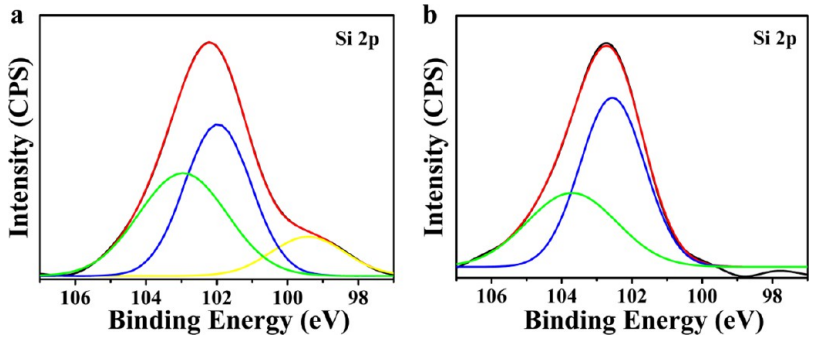

Figure 4. Deconvoluted Si 2p narrow scan spectra of hydrophobic silicon nanoparticle (a) and Si-HPG (b). The peaks at 99.4, 103, and 101.9 eV are due to Si(0), silicon oxide, and silicon capped with hydrophobic ligands, respectively. For Si-HPG, the peak for Si(0) at 99.4 eV disappears either due to the low XPS probing depth or shifting to higher binding energy by insulating HPG.

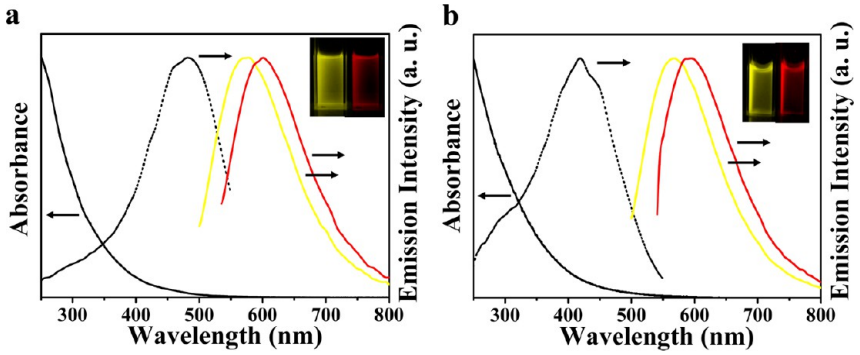

Figure 5. Absorption spectra (—), fluorescence excitation spectra (···), and fluorescence spectra (color lines) of a chloroform solution of hydrophobic silicon nanoparticles (a) and an aqueous solution of Si-HPG (b). Excitation spectra have been obtained using fluorescence at 570 nm and fluorescence spectra have been measured using 480 nm excitation (yellow line) and 515 nm excitation (red line). Inset shows the digital fluorescence images of the corresponding nanoparticles solutions.

(L_{14}) carbon (at 69.05 ppm corresponding to CHOH and at 72.29 ppm corresponding to CH_2) units of dendritic HPG are observed (Figure 3). The degree of branching (DB) of Si-HPG is estimated as 0.47 using the intensity ratio of respective ^{13}C NMR signals.[41] This result shows that dendritic HPG are effectively grafted on the silicon nanoparticle surface. The succinic acid functionalization of Si-HPG has been confirmed from the ^{1}H NMR spectrum of Si-HPG-COOH with the appearance of peak around 2.52 ppm due to methylene protons of succinic acid (Figure 3). In addition the proton peaks of $-CH_2O-$ and $-CHO-$ units of HPG are shifted a little bit after succinic acid functionalization. These results show that succinic acid is successfully conjugated with hydroxy groups of Si-HPG nanoparticles.

Fourier transform infrared (FTIR) spectra of hydrophobic silicon nanoparticles, Si-HPG and Si-HPG-COOH provide the signature of changed surface of nanoparticles (Supporting Information, Figure S5). The FTIR spectrum of hydrophobic silicon nanoparticles shows C−H stretching at 2960−2850 cm^{-1} and CH_2 bending at 1460 cm^{-1} corresponding to hydrophobic ligands and a strong band at 3450 cm^{-1} corresponding to surface hydroxy groups. The FTIR spectrum of Si-HPG shows the signature of HPG for stretching vibration of O−H, C−H, and C−O−C at 3420, 2880, and 1080 cm^{-1}, respectively. FTIR spectrum of Si-HPG-COOH displays an additional peak for C═O stretching vibration at 1731 cm^{-1} due to carboxy groups.

X-ray photoelectron spectroscopy (XPS) study has been performed to evaluate the elemental composition before and after HPG grafting. The wide scan XPS spectra of both hydrophobic silicon nanoparticle and Si-HPG show the photoelectron lines with binding energy of about 102, 154, 284, and 532 eV that are attributed to the presence of Si 2p, Si 2s, C 1s, and O 1s energy levels, respectively (Supporting Information, Figure S6). In order to confirm the nature of bonding, we further studied the narrow scan XPS spectra. The Si 2p narrow scan spectrum of hydrophobic silicon nanoparticle shows three components at 99.4, 101.9, and 103 eV that correspond to core Si(0), silicon with insulating hydrophobic ligands, and silicon oxide, respectively (Figure 4). The presence of long chain hydrophobic ligands in hydrophobic silicon nanoparticles is also confirmed from the C 1s narrow scan spectrum. Deconvoluted O 1s peaks of hydrophobic silicon nanoparticle at 530.7, 531.6, and 533.1 eV are assigned to Si−O, Si═O, and O−H bonds, respectively, indicating the presence of oxide and hydroxyl groups. In the case of Si-HPG, the deconvoluted Si 2p narrow scan spectrum at 102.5 and 103.7 eV are assigned as silicon with insulating ligands and silicon oxide, respectively, and the peak corresponding to Si(0) disappears possibly due to low XPS probing depth compared with the thickness of grafted HPG or shifting to higher binding energy due to the insulating HPG grafting that overlaps with the peaks at 102.5 and 103.7 eV.[24] In addition deconvoluted C 1s shows two peaks at 285.1 and 286.3 eV that are attributed to C−C/C−H and C−O−C/C−O−H, respectively. Similarly, deconvoluted O 1s shows three peaks at 530.1, 532.4, and 533.3 eV that are assigned for Si−O, C−O−C/C−O−H, and O−H, respectively.

The RGD peptide conjugation of Si-HPG-RGD has been tested by coupling reaction of 9,10-phenanthrenequinone with

dx.doi.org/10.1021/am406061x | ACS Appl. Mater. Interfaces 2014, 6, 4301−4309

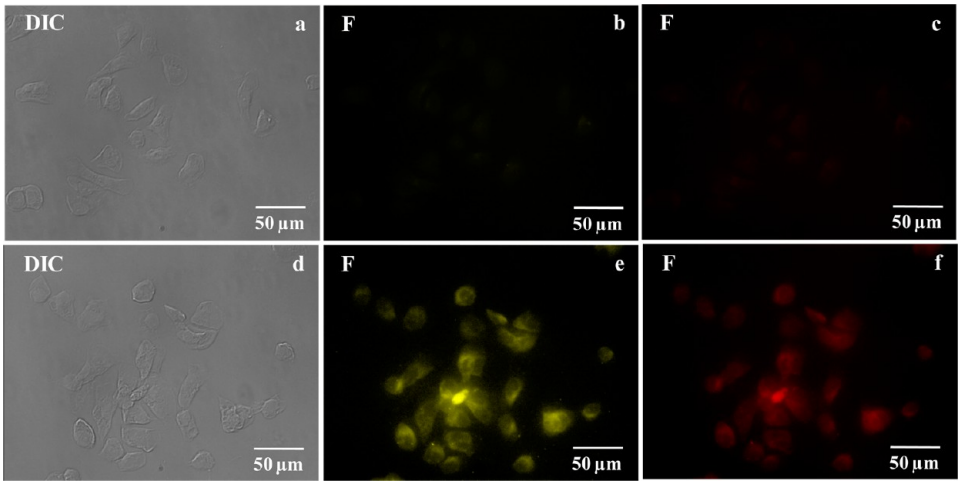

Figure 6. Differential interference contrast (DIC) and fluorescence (F) images of HeLa cells labeled with Si-HPG-RGD. Nanoparticles were incubated with HeLa cells at a final concentration of 0.8 mg/mL for 2 h (a, b, c) or 4 h (d, e, f) for the imaging study. For each row, the images from left to right shows the DIC images (a, d), fluorescence images under blue excitation (b, e), and fluorescence images under green excitation (c, f).

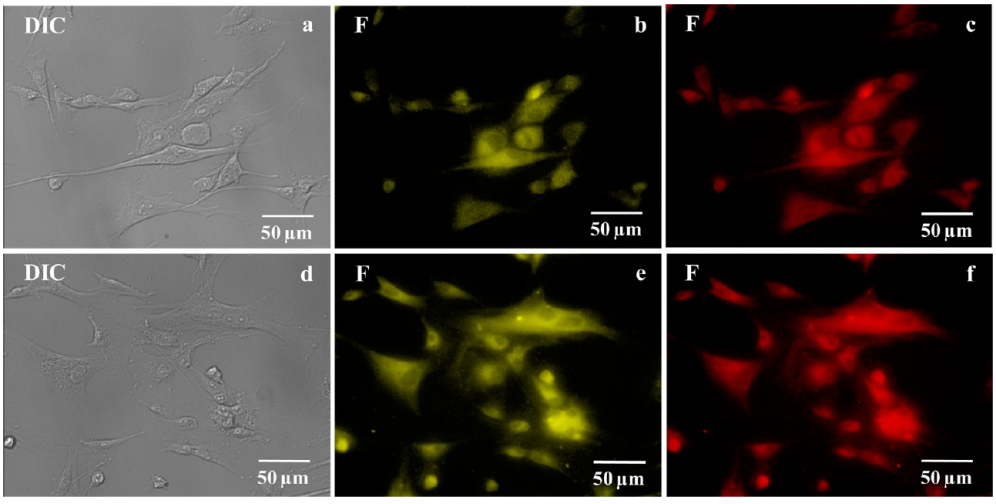

Figure 7. Differential interference contrast (DIC) and fluorescence (F) images of U87MG cells labeled with Si-HPG-RGD. Nanoparticles were incubated with U87MG cells at final concentration of 0.8 mg/mL for 2 h (a, b, c) or 4 h (d, e, f) for imaging study. For each row, the images from left to right shows the DIC images (a, d), fluorescence images under blue excitation (b, e), and fluorescence images under green excitation (c, f).

arginine present in the RGD peptide.[40] The reaction typically occurs at high pH followed by acidification that produces fluorescent molecule. The result shows that Si-HPG-RGD produces strong fluorescence at 400 nm in the presence of 9,10-phenanthrenequinone, while Si-HPG and Si-HPG-COOH show weak fluorescence under similar condition (Supporting Information Figure S7) This result suggests that RGD peptide is successfully conjugated with Si-HPG. We have also calculated the approximate concentration of RGD peptide present in the form of Si-HPG-RGD during the cellular labeling condition, and the concentration is typically ~0.2 mM.

The colloidal stability of Si-HPG has been tested at different pH and under high ionic strength (Figure 2 and Supporting Information Figure S8). Results show that a solution of Si-HPG is highly stable under those conditions for months without any turbidity or precipitation. The colloidal stability and fluorescence stability of Si-HPG have also been tested in biological medium such as in cell culture medium. The fluorescence of Si-HPG is stable for more than 4 months without any particle precipitation (Figure 2).

Optical properties of the silicon nanoparticles have been investigated by photoluminescence spectroscopy (Figure 5 and Supporting Information, Figure S9). Both the hydrophobic silicon nanoparticles and Si-HPG have excitation-dependent emission (Supporting Information, Figure S9). The emission maxima red shift from 500 to 630 nm as the excitation wavelength changes from 300 to 550 nm. However, they have most intense emission under 400−550 nm excitation with the broad emission ranging from 450 to 700 nm having excitation-dependent emission maxima in the range of 500−630 nm. The fluorescence quantum yield has also been measured before and after HPG grafting and lies between 6% and 9% (Supporting Information, Table S1). Fluorescence property has also been measured for Si-HPG-COOH and Si-HPG-RGD and remains similar to that of Si-HPG (Supporting Information, Table S1). Results suggest that HPG grafting and further functionalization do not significantly alter the fluorescence property of silicon nanoparticles. Moreover, the fluorescence of a film of Si-HPG does not bleach even after 10 min of continuous exposure with blue or green lights (Supporting Information Figure S10). This result suggests that fluorescence of Si-HPG would be stable for

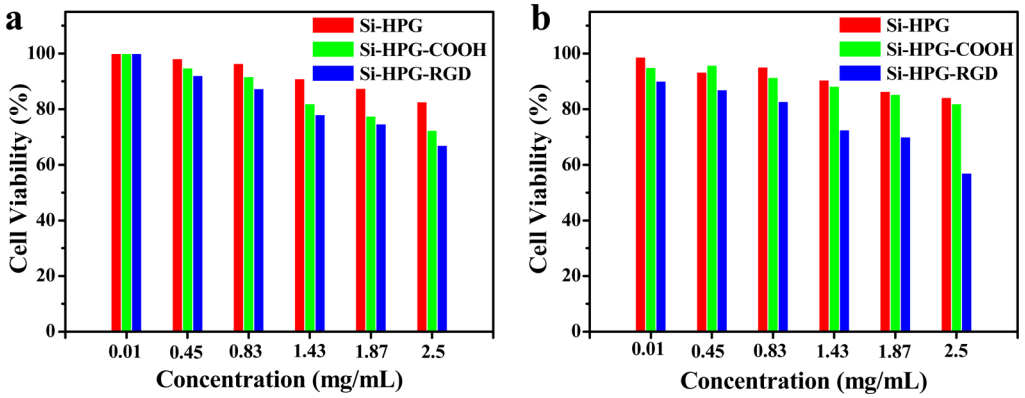

Figure 8. Viability of (a) HeLa and (b) U87MG cells after 24 h of incubation with Si-HPG, Si-HPG-COOH, and Si-HPG-RGD at different concentrations.

imaging based applications. The time-resolved fluorescence decay of hydrophobic silicon nanoparticles and Si-HPG demonstrate similar decay profiles (Supporting Information, Figure S11). The fluorescence decay of Si-HPG is fitted with three exponential lifetimes with an average lifetime of ∼4 ns and hydrophobic silicon nanoparticles also shows similar decay with an average lifetime of ∼3 ns. The fast recombination for both cases provides strong evidence that the origin of emission of silicon nanoparticles remains the same even after the HPG grafting.[21,33]

Yellow/Red/NIR Fluorescent Silicon Nanoparticle as Bioimaging Probe. The bioimaging application potential of fluorescent silicon nanoparticle has been investigated using Si-HPG-RGD toward targeting and imaging of cancer cells having overexpressed integrins. We have used HeLa (human cervical cancer) cells with low expression integrin $\alpha_v\beta_3$ and U87MG (human glioblastoma cells) with high expression of integrin $\alpha_v\beta_3$ for this study.[42] HeLa or U87MG cells were incubated with the solutions of silicon nanoparticles for 2−4 h, and washed cells were imaged under a fluorescence microscope. Fluorescence imaging was performed under blue excitation with the fluorescence signals collecting in the range of >520 nm or under green excitation with fluorescence signals collecting in the range of >590 nm. Figures 6 and 7 show that Si-HPG-RGD can successfully label HeLa and U87MG cells, and broad emission of silicon nanoparticles in the range of 450−700 nm can be used for imaging of cancer cells using yellow/red/NIR emission. However, labeling performance depends on cell type and incubation time. For example, fluorescence imaging of HeLa cells demonstrates that the uptake of the Si-HPG-RGD is negligible for 2 h of incubation and significant uptake requires an incubation time of >4 h. This is possibly due to low numbers of $\alpha_v\beta_3$ integrin on the cell surface that results in a slower uptake rate of Si-HPG-RGD and thus requires longer time for efficient labeling. In contrast, uptake of Si-HPG-RGD in U87MG cells is high at both 2 and 4 h of incubation. This is due to high numbers of $\alpha_v\beta_3$ integrin on the cell surface that leads to rapid uptake of Si-HPG-RGD by the cells (Figure 7). In both cells the Si-HPG-RGD appears to distribute in the cytoplasm. We have also tested the control labeling experiments with Si-HPG and Si-HPG-COOH, and results show that they have very little cell uptake (Supporting Information, Figure S12−S15). This result suggests that Si-HPG and Si-HPG-COOH have very low nonspecific binding to the cells and RGD acts as affinity molecule for cell targeting and uptake.

Biocompatibility of silicon nanoparticle-based nanoprobes was tested via MTT (3-(4,5-dimethylthiazol-2-yl)-2,5-diphenyltetrazolium bromide) based cytotoxicity assay using HeLa and U87MG cells. Silicon nanoparticles of different concentration were incubated with cells for 24 h, and then viability was compared assuming 100% viability for cells without nanoparticles. Figure 8 shows high viability of cells when they are exposed with various final concentrations (0.1−2.5 mg/mL) of silicon nanoparticles for 24 h. For example, cell viability is >80% in the concentration range of <1 mg/mL of Si-HPG, Si-HPG-COOH, and Si-HPG-RGD. In addition the cell viability is >80% for Si-HPG and Si-HPG-COOH at the highest concentration (2.5 mg/mL) tested. However, the cell viability is relatively low (60−70%) at 2.5 mg/mL of Si-HPG-RGD. Higher cell viability of Si-HPG and Si-HPG-COOH is due to their low nonspecific interaction with cells compared to Si-HPG-RGD that interact with cells and hinders the cell function.

Significance of Si-HPG Based Bioimaging Probe. The HPG-based coating of silicon nanoparticles reported here is unique as it transforms hydrophobic silicon nanoparticles into water-soluble nanoparticles with superior colloidal stability under high ionic strength and physiological medium. The grafting of polyglycerol has been combined with the synthetic approach of hydrophobic silicon nanoparticles in such a way that Si-HPG can be synthesized in one step and with complete conversion into water-soluble nanoparticles. The proposed approach has been used to prepare milligram scale synthesis of Si-HPG and can be extended to gram scale synthesis. Moreover we have demonstrated that terminal hydroxy groups can be used for further functionalization with different affinity molecules. The proposed approach can also be extended to other hydrophobic nanoparticles such as hydrophobic carbon, iron oxide, and quantum dot. The reported silicon nanoparticle-based imaging probe is unique for three reasons. First, the nanoprobe has emission in the red/NIR region that can be excited by blue and green light. Thus the nanoprobe can be used for deep tissue imaging applications. Second, the optimum hydrodynamic size of 25 nm is ideal for cellular and subcellular targeting. Third, nearly zero surface charge of the nanoprobe offers insignificant nonspecific interaction with cells. Thus these nanoparticles are ideal for specific targeting to cells after linking with affinity molecules.

Recently, various red/NIR fluorescent bioimaging nanoprobes have been reported, including QD, carbon nanoparticles, and europium-doped nanoparticles. Among them QD-based probes are most widely studied and more attractive due to their

dx.doi.org/10.1021/am406061x | ACS Appl. Mater. Interfaces 2014, 6, 4301−4309

narrow emission and high photostability.[5,43] However, heavy metals-associated toxicity limits their versatile applicability.[12,44] Although europium-doped nanoparticles have low toxicity, their fluorescence quantum yield is low, environment-dependent, and excitable under UV light, which limits their potential application.[45,46] Carbon nanoparticle-based probes enjoy low toxicity, but preparation of high quality red fluorescence probes is still scientifically challenging.[34,47] In these respects silicon nanoparticles are promising as they have low toxicity, high quantum yield, and high photostability. Presented polyglycerol grating and functionalization of silicon nanoparticle shows that various red fluorescent functional nanoparticles can be synthesized in large scale for different bioimaging applications.

CONCLUSION

In conclusion, we have synthesized hyperbranched polyglycerol grafted silicon nanoparticles of 25 nm hydrodynamic size that have red/NIR fluorescence. The nanoparticles have high water solubility and superior colloidal stability under physiological medium. The silicon nanoparticles have been transformed into functional nanoprobes with stable red/NIR fluorescence and have been successfully used as a fluorescent biological label. The low nonspecific binding with the cell, optimum particle size, and low toxicity present great potential of this nanoprobe for various *in vitro* and *in vivo* applications.

ASSOCIATED CONTENT

Supporting Information

Characterization details and data on control experiments. This material is available free of charge via the Internet at http://pubs.acs.org.

AUTHOR INFORMATION

Corresponding Author

*Fax: + 91-33-24732805. Tel: +91-33-24734971. E-mail: camnrj@iacs.res.in.

Notes

The authors declare no competing financial interest.

ACKNOWLEDGMENTS

The authors acknowledge CSIR, DST, and DBT, government of India for financial assistance. P.D. acknowledges CSIR, India for research fellowships. We acknowledge DST Unit of Nanoscience, IACS for their XPS facility.

REFERENCES

(1) Rao, J.; Dragulescu-Andrasi, A.; Yao, H. Fluorescence Imaging In Vivo: Recent Advances. *Curr. Opin. Biotechnol.* **2007**, *18*, 17−25.
(2) Kiyose, K.; Kojima, H.; Nagano, T. Functional Near-Infrared Fluorescent Probes. *Chem.−Asian J.* **2008**, *3*, 506−515.
(3) Escobedo, J. O.; Rusin, O.; Lim, S.; Strongin, R. M. NIR Dyes for Bioimaging Applications. *Curr. Opin. Chem. Biol.* **2010**, *14*, 64−70.
(4) Luo, S.; Zhang, E.; Su, Y.; Cheng, T.; Shi, C. A Review of NIR Dyes in Cancer Targeting and Imaging. *Biomaterials* **2011**, *32*, 7127−7138.
(5) Kim, S.; Lim, Y. T.; Soltesz, E. G.; Grand, A. M. D.; Lee, J.; Nakayama, A.; Parker, J. A.; Mihaljevic, T.; Laurence, R. G.; Dor, D. M.; Cohn, L. H.; Bawendi, M. G.; Frangioni, J. V. Near-Infrared Fluorescent Type II Quantum Dots for Sentinel Lymph Node Mapping. *Nat. Biotechnol.* **2004**, *22*, 93−97.
(6) Jin, Y.; Ye, F.; Zeigler, M.; Wu, C.; Chiu, D. T. Near-Infrared Fluorescent Dye-Doped Semiconducting Polymer Dots. *ACS Nano* **2011**, *5*, 1468−1475.
(7) Kumar, R.; Roy, I.; Ohulchanskky, T. Y.; Vathy, L. A.; Bergey, E. J.; Sajjad, M.; Prasad, P. N. In Vivo Biodistribution and Clearance Studies Using Multimodal Organically Modified Silica Nanoparticles. *ACS Nano* **2010**, *4*, 699−708.
(8) Wu, P.; Yan, X. P. Doped Quantum Dots for Chemo/Biosensing and Bioimaging. *Chem. Soc. Rev.* **2013**, *42*, 5489−5521.
(9) Kang, Z.; Liu, Y.; Lee, S. T. Small-Sized Silicon Nanoparticles: New Nanolights and Nanocatalysts. *Nanoscale* **2011**, *3*, 777−791.
(10) Medintz, I. L.; Uyeda, H. T.; Goldman, E. R.; Mattoussi, H. Quantum Dot Bioconjugates for Imaging, Labeling and Sensing. *Nat. Mater.* **2005**, *4*, 435−446.
(11) Basiruddin, S. K.; Saha, A.; Pradhan, N.; Jana, N. R. Advances in Coating Chemistry in Deriving Soluble Functional Nanoparticle. *J. Phys. Chem. C* **2010**, *114*, 11009−11017.
(12) Derfus, A. M.; Chan, W. C. W.; Bhatia, S. N. Probing the Cytotoxicity of Semiconductor Quantum Dots. *Nano Lett.* **2004**, *4*, 11−18.
(13) Fan, J.; Chu, P. K. Group IV Nanoparticles: Synthesis, Properties, and Biological Applications. *Small* **2010**, *6*, 2080−2098.
(14) He, Y.; Fan, C.; Lee, S. T. Silicon Nanostructures for Bioapplications. *Nano Today* **2010**, *5*, 282−295.
(15) Choi, J.; Zhang, Q.; Reipa, V.; Wang, N. S.; Stratmeyer, M. E.; Hitchins, V. M.; Goering, P. L. Comparison of Cytotoxic and Inflammatory Responses of Photoluminescent Silicon Nanoparticles with Silicon Micron-Sized Particles in RAW 264.7 Macrophages. *J. Appl. Toxicol.* **2009**, *29*, 52−60.
(16) Wang, J.; Sun, S.; Peng, F.; Cao, L.; Sun, L. Efficient One-Pot Synthesis of Highly Photoluminescent Alkyl-Functionalised Silicon Nanocrystals. *Chem. Commun.* **2011**, *47*, 4941−4943.
(17) Veinot, J. G. C. Synthesis, Surface Functionalization, and Properties of Freestanding Silicon Nanocrystals. *Chem. Commun.* **2006**, 4160−4168.
(18) Manhat, B. A.; Brown, A. L.; Black, L. A.; Ross, J. B. A.; Fichter, K.; Vu, T.; Richman, E.; Goforth, A. M. One-Step Melt Synthesis of Water-Soluble, Photoluminescent, Surface-Oxidized Silicon Nanoparticles for Cellular Imaging Applications. *Chem. Mater.* **2011**, *23*, 2407−2418.
(19) He, Y.; Zhong, Y.; Peng, F.; Wei, X.; Su, Y.; Lu, Y.; Su, S.; Gu, W.; Liao, L.; Lee, S. T. One-Pot Microwave Synthesis of Water-Dispersible, Ultra Photo- and pH-Stable, and Highly Fluorescent Silicon Quantum Dots. *J. Am. Chem. Soc.* **2011**, *133*, 14192−14195.
(20) Zhong, Y.; Peng, F.; Wei, X.; Zhou, Y.; Wang, J.; Jiang, X.; Su, Y.; Su, S.; Lee, S. T.; He, Y. Microwave-Assisted Synthesis of Biofunctional and Fluorescent Silicon Nanoparticles Using Proteins as Hydrophilic Ligands. *Angew. Chem., Int. Ed.* **2012**, *51*, 8485−8489.
(21) Warner, J. H.; Hoshino, A.; Yamamoto, K.; Tilley, R. D. Water-Soluble Photoluminescent Silicon Quantum Dots. *Angew. Chem., Int. Ed.* **2005**, *44*, 4550−4554.
(22) Sudeep, P. K.; Page, Z.; Emrick, T. PEGylated Silicon Nanoparticles: Synthesis and Characterization. *Chem. Commun.* **2008**, 6126−6127.
(23) Ge, J.; Liu, W.; Zhao, W.; Zhang, H.; Zhuang, X.; Lan, M.; Wang, P.; Li, H.; Ran, G.; Lee, S. T. Preparation of Highly Stable and Water-Dispersible Silicon Quantum Dots by Using an Organic Peroxide. *Chem.−Eur. J.* **2011**, *17*, 12872−12876.
(24) Ruizendaal, L.; Pujari, S. P.; Gevaerts, V.; Paulusse, J. M. J.; Zuilhof, H. Biofunctional Silicon Nanoparticles by Means of Thiol-Ene Click Chemistry. *Chem.−Asian J.* **2011**, *6*, 2776−2786.
(25) Wang, J.; Liu, Y.; Peng, F.; Chen, C.; He, Y.; Ma, H.; Cao, L.; Sun, S. A General Route to Efficient Functionalization of Silicon Quantum Dots for High-Performance Fluorescent Probes. *Small* **2012**, *8*, 2430−2435.
(26) Erogbogbo, F.; Yong, K. T.; Roy, I.; Xu, G. X.; Prasad, P. N.; Swihart, M. T. Biocompatible Luminescent Silicon Quantum Dots for Imaging of Cancer Cells. *ACS Nano* **2008**, *2*, 873−878.
(27) Erogbogbo, F.; Yong, K. T.; Hu, R.; Law, W. C.; Ding, H.; Chang, C. W.; Prasad, P. N.; Swihart, M. T. Biocompatible Magnetofluorescent Probes: Luminescent Silicon Quantum Dots

Coupled with Superparamagnetic Iron(III) Oxide. *ACS Nano* **2010**, *4*, 5131−5138.
(28) Erogbogbo, F.; Yong, K. T.; Roy, I.; Hu, R.; Law, W. C.; Zhao, W.; Ding, H.; Wu, F.; Kumar, R.; Swihart, M. T.; Prasad, P. N. In Vivo Targeted Cancer Imaging, Sentinel Lymph Node Mapping and Multi-Channel Imaging with Biocompatible Silicon Nanocrystals. *ACS Nano* **2011**, *5*, 413−423.
(29) Shen, P.; Ohta, S.; Inasawa, S.; Yamaguchi, Y. Selective Labeling of the Endoplasmic Reticulum in Live Cells with Silicon Quantum Dots. *Chem. Commun.* **2011**, *47*, 8409−8411.
(30) Ohta, S.; Shen, P.; Inasawa, S.; Yamaguchi, Y. Size- and Surface Chemistry-Dependent Intracellular Localization of Luminescent Silicon Quantum Dot Aggregates. *J. Mater. Chem.* **2012**, *22*, 10631−10638.
(31) Li, Z. F.; Ruckenstein, E. Water-Soluble Poly(acrylic acid) Grafted Luminescent Silicon Nanoparticles and Their Use as Fluorescent Biological Staining Labels. *Nano Lett.* **2004**, *4*, 1463−1467.
(32) Henderson, E. J.; Shuhendler, A. J.; Prasad, P.; Baumann, V.; Maier-Flaig, F.; Faulkner, D. O.; Lemmer, U.; Wu, X. Y.; Ozin, G. A. Colloidally Stable Silicon Nanocrystals with Near-Infrared Photoluminescence for Biological Fluorescence Imaging. *Small* **2011**, *7*, 2507−2516.
(33) Das, P.; Saha, A.; Maity, A. R.; Ray, S. C.; Jana, N. R. Silicon Nanoparticle based Fluorescent Biological Label via Low Temperature Thermal Degradation of Chloroalkylsilane. *Nanoscale* **2013**, *5*, 5732−5737.
(34) Bhunia, S. K.; Saha, A.; Maity, A. R.; Ray, S. C.; Jana, N. R. Carbon Nanoparticle-based Fluorescent Bioimaging Probes. *Sci. Rep.* **2013**, *3*, 1473.
(35) Maity, A. R.; Palmal, S.; Basiruddin, S. K.; Karan, N. S.; Sarkar, S.; Pradhan, N.; Jana, N. R. Doped Semiconductor Nanocrystal based Fluorescent Cellular Imaging Probes. *Nanoscale* **2013**, *5*, 5506−5513.
(36) Wilms, D.; Stiriba, S. E.; Frey, H. Hyperbranched Polyglycerols: From the Controlled Synthesis of Biocompatible Polyether Polyols to Multipurpose Applications. *Acc. Chem. Res.* **2010**, *43*, 129−141.
(37) Wang, L.; Neoh, K. G.; Kang, E. T.; Shuter, B.; Wang, S. C. Superparamagnetic Hyperbranched Polyglycerol-Grafted Fe_3O_4 Nanoparticles as a Novel Magnetic Resonance Imaging Contrast Agent: An In Vitro Assessment. *Adv. Funct. Mater.* **2009**, *19*, 2615−2622.
(38) Zhou, L.; Gao, C.; Xu, W.; Wang, X.; Xu, Y. Enhanced Biocompatibility and Biostability of CdTe Quantum Dots by Facile Surface-Initiated Dendritic Polymerization. *Biomacromolecules* **2009**, *10*, 1865−1874.
(39) Zhao, L.; Takimoto, T.; Ito, M.; Kitagawa, N.; Kimura, T.; Komatsu, N. Chromatographic Separation of Highly Soluble Diamond Nanoparticles Prepared by Polyglycerol Grafting. *Angew. Chem., Int. Ed.* **2011**, *50*, 1388−1392.
(40) Schmitt, A.; Schmitt, J.; Münch, G.; Gasic-Milencovic, J. Characterization of Advanced Glycation End Products for Biochemical Studies: Side Chain Modifications and Fluorescence Characteristics. *Anal. Biochem.* **2005**, *338*, 201−215.
(41) Sunder, A.; Hanselmann, R.; Frey, H.; Mü1lhaupt, R. Controlled Synthesis of Hyperbranched Polyglycerols by Ring-Opening Multibranching Polymerization. *Macromolecules* **1999**, *32*, 4240−4246.
(42) Hong, H.; Shi, J.; Yang, Y.; Zhang, Y.; Engle, J. W.; Nickles, R. J.; Wang, X.; Cai, W. Cancer-Targeted Optical Imaging with Fluorescent Zinc Oxide Nanowires. *Nano Lett.* **2011**, *11*, 3744−3750.
(43) Kairdolf, B. A.; Smith, A. M.; Stokes, T. H.; Wang, M. D.; Young, A. N.; Nie, S. Semiconductor Quantum Dots for Bioimaging and Biodiagnostic Applications. *Annu. Rev. Anal. Chem.* **2013**, *6*, 143−62.
(44) Sun, H.; Zhang, F.; Wei, H.; Yang, B. The Effects of Composition and Surface Chemistry on the Toxicity of Quantum Dots. *J. Mater. Chem. B* **2013**, *1*, 6485−6494.
(45) Escudero, A.; Calvo, M. E.; Rivera-Fernàndez, S.; de la Fuente, J. M.; Ocaña, M. Microwave-Assisted Synthesis of Biocompatible Europium-Doped Calcium Hydroxyapatite and Fluoroapatite Luminescent Nanospindles Functionalized with Poly(acrylic acid). *Langmuir* **2013**, *29*, 1985−1994.
(46) Sasidharan, S.; Jayasree, A.; Fazal, S.; Koyakutty, M.; Nair, S. V.; Menon, D. Ambient Temperature Synthesis of Citrate Stabilized and Biofunctionalized, Fluorescent Calcium Fluoride Nanocrystals for Targeted Labeling of Cancer Cells. *Biomater. Sci.* **2013**, *1*, 294−305.
(47) Tao, H.; Yang, K.; Ma, Z.; Wan, J.; Zhang, Y.; Kang, Z.; Liu, Z. In Vivo NIR Fluorescence Imaging, Biodistribution, and Toxicology of Photoluminescent Carbon Dots Produced from Carbon Nanotubes and Graphite. *Small* **2012**, *8*, 281−290.